Howard Hughes Medical Institute

Published as: *Nat Struct Mol Biol*. 2019 June ; 26(6): 407–414.

Receptor subtype discrimination using extensive shape complementary designed interfaces

Luke T. Dang[1,2,3,†], **Yi Miao**[4,5,6,†], **Andrew Ha**[7], **Kanako Yuki**[7], **Keunwan Park**[8], **Claudia Y. Janda**[4,5,6,10], **Kevin M. Jude**[4,5,6], **Kritika Mohan**[4,5,6], **Nhi Ha**[7], **Mario Vallon**[7], **Jenny Yuan**[7], **José G. Vilches-Moure**[9], **Calvin J. Kuo**[7], **K. Christopher Garcia**[4,5,6,*], and **David Baker**[1,2,3,*]

[1]Department of Biochemistry, University of Washington, Seattle, Washington 98105, USA [2]Institute for Protein Design, University of Washington, Seattle, Washington 98105, USA [3]Howard Hughes Medical Institute, University of Washington, Seattle, Washington 98105, USA [4]Department of Molecular and Cellular Physiology, Stanford University School of Medicine, Stanford, California 94305, USA [5]Department of Structural Biology, Stanford University School of Medicine, Stanford, California 94305, USA [6]Howard Hughes Medical Institute, Stanford University School of Medicine, Stanford, California 94305, USA [7]Department of Medicine, Division of Hematology, Stanford University School of Medicine, Stanford, California 94305, USA [8]Systems Biotechnology Research Center, Korea Institute of Science and Technology, Gangneung 25451, Republic of Korea [9]Department of Comparative Medicine, Stanford University School of Medicine, Stanford, California 94305, USA [10]Present address: Princess Máxima Center for Pediatric Oncology, Utrecht, the Netherlands.

Abstract

Discriminating between closely related members of a protein family which differ at a limited number of spatially distant positions is a challenge for drug discovery. We describe an approach for computationally designing binders targeting functional sites with large, shape complementary interfaces to ‘read out’ subtle sequence differences for sub-type specific antagonism. Repeat proteins are computationally docked against a functionally relevant region of the target protein surface that varies in the different subtypes, and the interface sequences are optimized for affinity and specificity first computationally and then experimentally. We used this approach to generate a series of human Frizzled (Fz) subtype-selective antagonists with extensive shape complementary interaction surfaces considerably larger than those of repeat proteins selected from random

[*]Correspondence to: K.C.G. (kcgarcia@stanford.edu) and D.B. (dabaker@uw.edu).

Author contributions: L.T.D., Y.M., K.C.G. and D.B. conceived the project. L.T.D. computationally designed, optimized and characterized DRPB_Fz8, obtained SSM data for specificity tuning. Y.M. constructed Fz4/7 targeting library, performed yeast surface display selection, purified all proteins, determined complex structures and performed cell line DRPB inhibition assays. A.H., K.Y. and N.H. performed duodenum organoid experiments and *in vivo* histology experiments. J.G.V. contributed to tissue collection and pathology assessment. M.V. and J.Y. packaged adenovirus. K.P. contributed to computational DRPB design. C.Y.J. generated Luciferase reporter cell line. K.M.J. contributed to crystallography data collection. K.M. contributed to yeast surface display selections. C.J.K. supervised the organoid experiments and *in vivo* experiments. K.C.G. and D.B. supervised the project and interpreted the data. L.T.D., Y.M., K.C.G. and D.B. wrote the manuscript with inputs from all authors.

[†]These authors contributed equally: Luke T. Dang and Yi Miao

Competing interests: K.C.G., D.B., Y.M. and L.T.D. are inventors on patent applications 62/698576 submitted by Stanford University that covers the use of Frizzled specific Wnt antagonists.

libraries. In vivo administration revealed that Wnt-dependent pericentral liver gene expression involves multiple Fz subtypes, while maintenance of the intestinal crypt stem cell compartment involves only a limited subset.

A frequently encountered challenge in drug discovery is targeting a small subset of the members of a closely related protein family to achieve a specific therapeutic outcome with minimal off-target toxicity[1]. For example, cytokine and growth factor receptor systems (e.g. Interferons, Wnt, Notch, BMP, etc)[2–6] often have multiple receptor subtypes with different biological roles. Current strategies for targeting specific receptor or ligand sub-types generally involve selection from randomized libraries utilizing counter-screening for desired specificity[7,8]. Using these methods, high affinity Ankyrin binders called DARPins have been selected against a number of targets and show potential as therapeutics[9,10]. While capable of obtaining high affinity binders, library selection methods remain empirical, and cannot explicitly target specific regions of a protein surface. Previous efforts to generate specific binders against similar targets has therefore required the independent evolution of binders against each target[7,8]. An alternative, potentially superior strategy would be to target specific regions of a protein surface that could enable “reading out” of specificity between closely related homologues.

We reasoned that binding modes with extensive interface surfaces that span spatially distant variant positions could provide a general solution to the problem of discriminating between closely related members of a protein family. We developed a two-step approach for designing binding modes poised for high affinity and specificity functional antagonism. First, we used computational design to target binding to a defined, large surface region of a family member structure that includes both the conserved functional site and adjacent non-conserved residues. This computational sampling of structure space can survey the wide range of possible backbone orientations more broadly than selection methods due to library size constraints. Second, we generated subtype specific variants by exploiting contacts with subtype specific positions within this broadly conserved buried surface. We chose repeat proteins as scaffolds due to their modular, idealized architecture, which enables extension as needed for the design of larger interfaces. In addition, the favorable biochemical properties of these designed repeat protein binders (DRPBs) are ideal for downstream functional applications.

Results

Computational design of Fz-subtype specific designed repeat protein binders (DRPBs).

We tested this approach on the Frizzled (Fz) family of Wnt receptors, an important example of a closely related set of therapeutic targets since sub-type specific antagonism of Fz could reduce or limit off-target toxicity[11]. Dysregulation of Wnt signaling is widely implicated in cancer[12]. However, full elucidation of the role of the Wnt pathway in tissue homeostasis and disease has been limited by the availability of reagents which can modulate signaling in a receptor subtype specific manner as there are 19 distinct Wnt ligands and 10 Fz receptors (as well as other co-receptors, inhibitors, and agonists)[11,13]. Different tissues express different subsets of Fz, so molecules are needed with the ability to distinguish between Fz sub-types

that are highly homologous in sequence. Indeed, highly cross-reactive anti-Fz monoclonal antibodies have been tested in clinical trials for several cancers but resulted in dose-limiting toxicity, including bone fractures (OncoMed Pharmaceuticals). Native Wnts do not provide good starting points for generating such binding reagents as they exhibit binding promiscuity for the different Fzs[14,15]. Furthermore, endogenous Wnts are lipidated, and not water-soluble, making them impractical to re-engineer for functional applications. We reasoned that the discrimination of subtle sequence differences between different Fzs (Fig. 1a, 1b, Supplementary Notes, page 18) could be achieved using repeat proteins such as Ankyrins which have extended concave surfaces roughly complementary to the convex surface adjacent to the lipid binding cleft of the Fz Cysteine-Rich Domain (CRD) structure[9,15].

We therefore sought to develop high-affinity subtype-specific Fz binders with extensive interfaces that included primary contacts with both the conserved lipid-binding cleft (to enable Wnt antagonism) as well as secondary contacts against adjacent positions which are variable between receptor subtypes (to enable development of orthogonal binding specificities). As random library selection methods do not enable such precise targeting (Fig. 1c), we utilized computational docking and design methods starting from an idealized Ankyrin scaffold (PDB:4GPM) previously optimized using Rosetta (each repeat is identical in this design, and it is very stable; because it is designed using Rosetta it has very low energy in the Rosetta force field which makes the subsequent interface design calculations more straightforward as energy optimization will change the sequence only to make new interactions with the target)[16,17]. The scaffold was globally docked against the Fz8 surface, and binding modes that inserted loops into the Wnt lipid binding groove and encompassed adjacent variable regions, had large interface surface areas and high backbone shape complementarity were selected. The interfaces of selected binding conformations were computationally optimized for low energy interactions with Fz8CRD. 22 designs with high shape-complementarity (average SC of 0.70) and extensive buried surface area (BSA) size (average >2400 AÅ^2) (Fig. 1d, 1e, Supplementary Notes, page 27) were chosen for experimental characterization. As we reasoned that there was a possibility of design errors over the extensive buried interface which could limit initial binding detection, we screened for Fz binding through error-prone PCR libraries via yeast surface display[18,19]. Following further sequence optimization, a final clone DRPB_Fz8 specifically bound Fz5 with a K_d of 220 pM as measured by biolayer interferometry (BLI) (Supplementary Notes, pages 19 and 30), competed for Fz binding with a previously designed protein, B12[20] and an anti-Fz scFv[14] (. Supplementary Notes, page 20), and is thermostable to 80 °C (Supplementary Notes, page 19); DRPB_Fz8 has essentially equal affinity for the very closely related Fz5 and Fz8 (Supplementary Fig. 1, and Supplementary Notes, page 33) and we used them interchangeably in these initial binding and optimization experiments depending on availability).

DRPB_Fz8-Fz8CRD complex structure confirms computational design and paves the way for specificity tuning.

To confirm our design, a 2.3 Å structure of the DRPB_Fz8-Fz8CRD complex was solved, revealing a binding mode virtually identical to the “fingers-in-groove” or “grasping-hand” design model (backbone RMSD 1.6 Å). This interaction fully occludes the Fz lipid binding

groove, preventing binding to the native Wnt lipid (Fig. 2, Supplementary Fig. 1). A difference between the DPRB_Fz8-Fz8CRD crystal structure and the original computational model is a narrowing of the receptor cleft upon binding due to shifting of the adjacent Fz alpha helix. Although it was accommodated in the computational model, Phe42 is incompatible with the narrowed conformation of the helical backbone in the crystal structure (Supplementary Fig. 1d); removing this bulky hydrophobic group restores the underlying designed high-affinity interface. The single point mutations Phe42Ala or Thr66Ser was sufficient to confer weak binding activity on the design, and the double substitution led to high affinity binding (Supplementary Fig. 1a).

We subsequently redesigned DRPB_Fz8 for specific binding to the other two major Fz subtypes, Fz1/2/7 and Fz4 utilizing a targeted library approach. To guide library construction, we built comparative models for Fz4/7 using Rosetta, aligned them to Fz8 in the DRPB_Fz8-Fz8CRD crystal structure, and carried out Rosetta design calculations to identify amino acid substitutions on DRPB_Fz8 that increase affinity for Fz4/7. In parallel, we generated a site saturation mutagenesis library containing point mutations to all residues of DRPB_Fz8, carried out selection towards Fz4 and Fz7, and identified enriched positions via next-generation sequencing (Supplementary Notes, pages 21–22)[19]. Substitutions suggested by both the computational and experimental data were integrated to generate focused libraries targeting Fz4/7 subtypes (Supplementary Notes, pages 31–32). Sorting of the Fz7 subtype yeast library yielded a biased, yet cross-reactive clone named DRPB_Fz7/8. (Fig. 3a and Supplementary Fig. 2). A further Fz7 subtype specific clone (Fig. 3b, Supplementary Notes, page 23) was isolated from an error-prone yeast library based on the DRPB_Fz7/8 scaffold. We used the same approach to select a Fz4 subtype specific DRPB. This structure guided library directly enriched as several clones, including the highly selective DRPB_Fz4 (Supplementary Notes, page 24), with a K_d of 1.4 nM to Fz4 (Fig. 3c, Supplementary Notes, page 23–25, Supplementary Fig. 3).

Complex structures of DRPB-Fz explain Fz subtype specificity

To dissect the molecular mechanism of DRPB affinity and specificity tuning, we determined the structures of all DRPB-FzCRD complexes (Fig. 3 and Table 1). Structural superposition of DRPB_Fz8-Fz8CRD with DRPB_Fz7/8-Fz7CRD revealed a key Ala111Asp mutation from DRPB_Fz8 to DRPB_Fz7/8, enabling appropriate hydrogen bond and salt bridge formation with a corresponding Lys of Fz7, which is a Glu in the Fz8 subtype (Fig. 3a, Supplementary Fig. 4a,b). The structure of Fz7-specific DRPB_Fz7 with Fz7CRD highlighted a Ala108Asp mutation, which clashes into Trp73 in the Fz8 subtype whilst this mutation is tolerated due to smaller sidechain of Tyr in Fz7 subtype (Fig. 3b, Supplementary Fig. 4c), explaining the enhanced specificity. The complex structure of DRPB_Fz4 in Fz4 CRD reveals a limited repositioning of DRPB_Fz4 compared with DRPB_Fz8, albeit with a globally preserved binding mode (Fig. 3c, Supplementary Fig. 5). Detailed structural analysis revealed that a combination of residues modulate this specificity change. Collectively, we have engineered DRPB antagonists to three major Fz subtypes using a designed, functionally targeted binding mode with high shape-complementarity and large BSA area, allowing us to distinguish between Fz isoforms. The successful reengineering of

binding specificity marks significant progress towards development of a suite of proteins with orthogonal binding specificities utilizing a pre-designed binding mode.

Fz-subtype specific DRPB antagonists inhibit homeostasis of the intestinal crypt stem cell compartment and expression of liver Wnt target genes.

Despite pleiotropic involvement of Wnt signaling in stem cell biology and tissue homeostasis, genetic redundancy between the 10 Fzd genes has greatly hindered the identification of essential Fz gene(s) functionality in adult tissue compartments[11,13]. Therefore, systematic Fz subtype-specific inhibition, as with the DRPB antagonists, represents a robust pharmacologic solution to the quandary of functional interrogation of Fzd receptors *in vivo*. $Lgr5^+$ intestinal stem cells predominantly express Fz5 and Fz7, and to a lesser degree Fz1/2/6/8/9[21]; this redundancy likely underlies the inability of any single or combinatorial Fzd knockout to demonstrate an adult homeostatic intestinal phenotype.

To probe the Fz-subtype specific antagonist function of these DRPBs, we first treated cell lines with predominant expression of Fz2, 4 or 5 with DRPBs while stimulating with Wnt3a conditioned media. These Fz-selective DRPBs showed potent Fz-subtype specific inhibition of Wnt signaling, as demonstrated by TopFlash reporter (Supplementary Fig. 6). We then assessed the antagonist function of DRPBs during *in vitro* intestinal organoid growth. Since duodenal organoids produce endogenous Wnts, which are essential for their growth, organoid growth is a stringent readout for DRPB inhibitory activity. Both human and mouse duodenum organoid cultures were cultured with all four types of DRPBs. Both DRPB_Fz4 and DRPB_Fz7 showed no effects (Fig. 4a). DRPB_Fz8 strongly inhibited organoid growth in the 0.1–1 nM range, but several log higher concentrations of DRPB_Fz7/8 was required (Fig S7a,b), consistent with the stronger Fz affinity of DRPB_Fz8 versus DRPB_Fz7/8 (Supplementary Fig. 3). For *in vivo* studies we fused the DRPBs to mouse serum albumin (MSA) to extend circulating half-life. Notably, daily intravenous administration of MSA-DRPB_Fz8 but not the other DRPBs induced profound loss of crypts and villi within 7 days (Fig. 4b, Supplementary Fig. 7), consistent with blockade of canonical Wnt signaling via Dkk1 or Porcupine inhibitors[21–23]. We reasoned that the lack of effect of MSA-DRPB_Fz7/8 on duodenal homeostasis could be due to lower Fz binding affinity versus MSA-DRPB_Fz8 as reflected in organoid culture. To overcome this, we generated recombinant adenoviruses expressing each of the DRPBs, since intravenous adenovirus injection infects the mouse liver and allows continuous high-level hepatic secretion of transgene products into the circulation for weeks[21,24]. Accordingly, adenoviruses expressing DRPB_Fz7/8 and DRPB_Fz8 both produced rapid duodenal crypt/villus loss resulting in weight loss and lethality within 7 days, while DRPB_Fz4 and DRPB_Fz7 were ineffective despite robust serum expression of each DRPB (Fig. 4c and Supplementary Fig. 8). The ability of the restricted spectrum DRPB_Fz8 to elicit catastrophic crypt and villus loss strongly implicates Fz5 and/or Fz8 function during intestinal homeostasis with much stronger phenotypes that have been observed with individual Fz receptor genetic deletion[25].

The liver represents an additional Wnt-sensitive compartment, with Wnt pathway gain- or loss-of-function profoundly altering zonated expression of liver genes[20,26]. Adenoviruses expressing each of the four DRPBs, or negative control adenovirus were tested for effects on

the Wnt-responsive genes Glul (glutamine synthetase) and Axin2. While negative control adenovirus liver (Adeno-Fc) expressed GLUL in a highly characteristic pericentral zone, adenovirus-expressed DRPB_Fz4, DRPB_Fz7 and DRPB_Fz8 partially repressed GLUL, and notably DRPB_Fz7/8 completely repressed GLUL (Fig. 4d, e). This was strongly paralleled by the complete repression of liver *Glul* and *Axin2* mRNA by DRPB_Fz7/8 with more intermediate inhibition seen with DRPB_Fz4, DRPB_Fz7 and DRPB_Fz8 (Fig. 4f, g). Thus, in contrast to the comparatively narrow Fz functional spectrum of intestinal homeostasis, Wnt dependent liver gene expression appears to require the broad-based contribution of diverse Fz receptor subtypes. In such a manner, our strategy enables 'tuning' Fz specificity based on tissue expression of the Fz sub-types.

Discussion

It is instructive to compare the structure of our designed complex to those of DARPin-protein complexes obtained using library selection methods. The binding interface in the DPRB-target designed complex is significantly larger compared to single domain DARPin-protein complexes in the Protein Data Bank (PDB) (Fig. 1d); despite the much larger surface area, the overall shape complementarity is very similar. Large shape complementary interfaces are difficult to obtain by traditional random library selection as only a small fraction of the available sequence space can be searched, and hence favorable interactions throughout the interface are much less likely than for smaller interfaces. The difficulty of empirically selecting interfaces with such large surface area becomes clear when considering the increase in combinatorial diversity accompanying increasing interface size. For example, the DPRB initially designed here has 32 interface contacting residues mutated from the original scaffold. A full coverage library sampling these positions that includes all twenty amino acids at each site would represent a diversity of 20^32 or 4.29E41, dwarfing the screening capabilities of current yeast, phage or ribosome display methods. Libraries in which only a subset of the interface residues are varied can be made, but several of the residues kept constant are likely to be incompatible with binding, and hence large interfaces are unlikely to be obtained by selection. Computation can explicitly identify binding modes with large shape complementary interfaces, and optimize the sequence to be complementary to the target surface (while powerful, this approach is not free of the challenges associated with large interfaces as illustrated by the inclusion of the problematic Phe in the initial design). The designed binding mode, with "hand-in-groove" insertion of ankyrin loops into the Fz lipid binding groove, is well suited to distinguish between closely related Fz subtypes with high affinity due the large, hydrophobic interface which makes contacts with both spatially disparate variant residues and core conserved regions. The principal advantages of our approach over traditional selection methods are (1) the ability to generate much larger shape complementary binding interfaces and (2) the ability to target these binding interfaces to functional regions encompassing sequence diversity among receptor sub-types.

Our design protocol can be broadly generalized to other ligand-receptor or protein-protein systems, with particular utility for challenging applications where high affinity binding is insufficient and specific backbone placement is required for functional activity and specificity. The use of repeat proteins facilitates the design of custom binders with extensive interfaces to specification in such cases. Specific pharmacologic inhibition of these Wnt

receptors by our approach provides a dose-dependent, robust tool for precise interrogation of Wnt signaling in a range of key processes. For instance, while redundancy has complicated the association of the 10 distinct Frizzled genes with specific biological processes, our studies suggest predominant relevance of Fz5 and/or Fz8 to intestinal stem cell homeostasis but broad contributions of multiple Fz receptors to Wnt-driven liver zonation. Knockout studies have previously demonstrated a critical role for Fz5 and Fz8 in mouse retinal development, but the Fz5 and Fz8 double knockout is embryonic lethal[27], limiting further detailed study. This proof of principle marks significant progress in the combined application of computational design and selection methods towards the development of protein-protein interfaces which enable the molecular recognition of closely related proteins for the elucidation of complex signaling networks and precise therapeutic intervention minimizing off-target effects.

Methods

Computational design and in vitro evolution by yeast surface display

Due to space considerations of the Methods section, the detailed protocol is included in the Supplementary Notes.

Biolayer Interferometry

Data was collected with an Octet RED96 (FortéBio, Menlo Park, CA, USA) instrument and analyzed with the ForteBio data analysis package. All experiments were performed at room temperature in HBS-EP Buffer (GE Biosciences) with bovine serum albumin (BSA) blocking agent added (0.01 M HEPES, pH 7.4, 0.15 M NaCl, 3 mM EDTA, 0.005% v/v Surfactant P20, 1% BSA). Dip and Read Streptavidin Biosensors (ForteBio) were activated for 30 minutes in buffer prior to loading with biotinylated Fz5CRD (at 50 nM). After baseline reference collection, biosensors were dipped in analyte binder solutions to measure association and then returned to the empty buffer-containing baseline well to measure dissociation. Kinetic binding constants were determined after reference subtraction utilizing a 1:1 binding model. Competition assays were carried out by loading the biosensors with biotinylated protein and then sequentially subjecting the biosensors to 250 nM (in HBS-EP Buffer) of protein A and then B (DRPB_Fz8, B12, Oncomed scFv or buffer)[28,29].

Circular Dichroism

DRPB_Fz8 was dialyzed into PBS (20mM $NaPO_4$, 150mM NaCl) and analyzed at a final concentration of 12 mg/mL. Circular dichroism (CD) spectra were collected on an AVIV Model 420 CD spectrometer (AVIV Biomedical, Inc, Lakewood, NJ, USA) using a 1 mm pathlength quartz cuvette. Scans were collected at 25°C and were taken from 195 to 265 nm in 1 nm steps with 1 nm bandwidth at a scanning speed of 10 nm/minute. Three independent scans were averaged and buffer subtracted against a cuvette holding PBS. Temperature melts were carried out with the same parameters from 25°C to 95°C in 1°C steps reading at 222 nm. During the melt, a full wavelength scan was taken at 25, 35, 45, 55, 65, 75, 85, and 95°C using the parameters above.

Protein constructs, expression and purification

All the DPRB protein sequences were cloned with a C-terminal His-tag into pET28a vector. The vectors were transformed into BL21(DE3)pLysS cells (Life Technologies) and induced by 0.5 mM IPTG at 16 °C for 16 h when the OD_{600} reached 0.6. Cells were pelleted by centrifugation and lysed by sonication in lysis buffer (20 mM HEPES, pH 7.2, 300 mM NaCl). The proteins were purified by Ni^{2+}-Nitrolotriacetic acid (NTA) affinity column chromatography followed by size exclusion chromatography via a Superdex S75 column (GE Healthcare) in HBS buffer (10 mM HEPES, pH 7.2, 150 mM NaCl). The Mouse Serum Albumin (MSA)-DRPB proteins were expressed in High Five (*Trichoplusia ni*) cells (Invitrogen) using the baculovirus expression system. These proteins were purified using Ni^{2+}-NTA affinity column chromatography followed by size exclusion chromatography via a Superdex S200 column (GE Healthcare) in PBS buffer. Subsequently, endotoxin was removed following instruction of Proteus NoEndoTM High Capacity Midi spin column kit (GEN-NoE12HC). Before administration, endotoxin levels were quantified by Pierce™ LAL Chromogenic Endotoxin Quantitation Kit (Catalog # 88282). The proteins were also sterile filtered.

The CRDs of human FZ1 (residues 113–182), FZ4 (residues 42–161), FZ7 (residues 36–163) and FZ8 (residues 32–150 with N49Q mutation) used for crystallization contained a C-terminal 6X His tag were expressed in High Five (*Trichoplusia ni*) cells (Invitrogen) using the baculovirus expression system. All proteins were secreted from High Five insect cells grown in Insect-Xpress medium, and purified using Ni^{2+}-NTA affinity column chromatography followed by size exclusion chromatography via a Superdex S75 column in HBS buffer. Similarly, The CRDs of these human FZDs were cloned with a C-terminal 3C protease cleavage site (LEVLFQ/GP), a biotin acceptor peptide (BAP)-tag (GLNDIFEAQKIEWHE) and a 6×His-tag and purified as described. These CRDs were site-specifically biotinylated using BirA biotin-protein ligase standard reaction kit (Avidity Catalog # BirA500). Successful biotinylation were confirmed by SDS-PAGE running Fz CRD side by side with Fz CRD mixed with SA.

Affinity measurements by Surface Plasmon Resonance

Biotinylated Fz CRDs were coupled on a SA sensor chip (GE Healthcare) at low density with target RU increase of 120. An unrelated biotinylated protein was captured at equivalent coupling density to the control flow cells. Increasing concentrations of DRPB proteins were flown over the chip in HBS-P buffer (GE Healthcare) containing 10% glycerol and 0.05% BSA at 30 μl/mL. The chip surface was regenerated after each injection with 4 M $MgCl_2$. The measurements were conducted using a BIAcore T100 (GE Healthcare) and analyzed by the accompanying evaluation software.

Protein crystallization, data collection and structure determination and refinement

Individual DRPB-Fz CRD complex was formed by mixing purified protein in 1:1 ratio. The complex was further treated with 1:100 (w/w) carboxypeptidase A (Sigma # C9286) and carboxypeptidase B (Sigma # C9584) for overnight at 4°C. The complex was further purified by size exclusion chromatography via a Superdex S75 column (GE Healthcare) in

HBS buffer. The purified complex was concentrated using an Amicon Ultra concentrator (10K MWCO, Millipore). Crystals were grown by sitting-drop vapor diffusion at 295 K.

The DRPB_Fz8-Fz8CRD complex protein was concentrated to 40 mg/mL in HBS buffer. Crystals showed up after one month in 0.2 M ammonium acetate, 0.1 M HEPES, pH 7.5 and 55% MPD. The DRPB_Fz4-Fz4CRD complex protein was concentrated to 40 mg/mL in HBS buffer. Crystals showed up after two weeks in 0.2 M ammonium chloride, pH 6.3 and 20% PEG 3,350. The DRPB_Fz7/8-Fz7CRD complex protein was concentrated to 14 mg/mL in HBS buffer. Crystals showed up after 5 days in 0.1 M sodium acetate, pH 4.5, 2 M ammonium sulfate. The DRPB_Fz7-Fz7CRD complex protein was concentrated to 20 mg/mL in HBS buffer. Crystals showed up after one week in 0.2 M Na_2HPO_4: citric acid, pH 4.2 and 2M Ammonium sulfate.

X-ray intensity data sets were collected at the Advanced Light Source (ALS) 8.2.1 and 8.2.2 lines, Advanced Photon Source (APS) 23-ID-D line and Stanford Synchrotron Radiation Lightsource (SSRL) 12–2 line. Data were indexed and scaled using XDS[30] or HKL 2000[31]. The DRPB_Fz8-Fz8 CRD structure with was determined by molecular replacement using Phaser. The Rosetta calculated DRPB_Fz8 structure and the Fz8 CRD (PDB code: 4F0A[32]) structure were used as the search models. Similarly, the other structures were determined using their respective Fz CRD model (PDB code: 5BPB and 5T44). All structures were manually built in Coot[33] and improved by multiple rounds of refinement in Phenix[34] and manual rebuilding. Detailed statistics for data collection and refinement were reported in Table 1. These structures are deposited at the Protein Data Bank (PDB) under the accession codes: 6NDZ, 6NE1, 6NE2 and 6NE4, with 97.3%, 95.6%, 98.4% and 98.1% Ramachandran favored residues and none Ramachandran outliers, respectively.

Fz-specific Inhibition using Luciferase Assay

HEK293T and A375 cells were stably transfected with the luciferase reporter and a constitutively expressed *Renilla* luciferase as previously reported[28], denoted as HEK293STF and A375BAR. BeWo cells were stably transfected with lentiviral transfection expressing firefly luciferase reporter as previously described[28]. The assay measurement were performed using the Dual Luciferase Assay kit (Promega # E1960) as instructed. A375BAR cell line was used as Fz2 predominant cell line and BeWo (ATCC) cell line was used as Fz5 predominant cell line. Briefly, 10,000 to 20,000 cells were plated to each well in a 96-well sterile cell culture plate for overnight. The next day, cells were pre-incubated with a increasing concentration of DRPBs for 1 hr. The cells were subsequently stimulated with 20% Wnt3a conditioned media (ATCC) with 25 nM R-spondin protein for another 20 hrs. In Fz4 inhibition assays, a Fz4 predominant cell line was difficult to isolate. Therefore, HEK293STF cells were plated at a density of 15,000 cells/well the first day. On the second day, the cells were transfected with human Fz4 receptor using Fugene HD (Promega) following manufacture's protocol. On the third day, the cells were pre-incubated with 20 nM DRPB_Fz7/8 (previously shown to fully inhibit Fz1/2/5/7/8 mediated Wnt signaling) and gradient concentration of DRPB_Fz4 for 1 hr. Therefore, the Luciferase signaling output in these cells were only mediated by Fz4 receptors. The cells were subsequently stimulated with 20% Wnt3a conditioned media and 25 nM R-spondin for another 20 hrs before

analysis. These cells were washed with PBS buffer (Thermo Fisher # 10010023) and lysed as instructed in the Dual Luciferase Assay kit (Promega) user manual. Luminance signals were recorded using SpectraMax Paradigm. The data were analyzed by Prism 7.

Organoid culture assay

Mouse duodenal organoids were derived from adult C57BL/6J mice (Jackson Laboratory, ME, USA) using the method described before[35]. Human duodenal organoids were established from de-identified surgical discards. Primary tissues were obtained through the Stanford Tissue Bank from patients undergoing surgical resection at Stanford University Medical Center (SUMC). All experiments utilizing human material were approved by the SUMC Institutional Review Board. Written informed consent for research was obtained from donors prior to tissue acquisition. For the 3D cultures, Matrigel (BD Biosciences) was used and overlaid with a liquid medium consisting of DMEM/F12 advanced medium (Invitrogen), supplemented with additional factors including EGF (50ng/ml), Noggin (100ng/ml), and RSPO (500ng/ml). Medium was replenished every 3 days.

In vivo experiments

Adult C57BL/6J mice (Jackson Laboratory, ME, USA) between 9–10 weeks old were injected intravenously with recombinant proteins (15mg/kg) or adenoviruses (doses of 1×10^9 pfu per mouse). Intestinal tissues were collected and fixed in 4% paraformaldehyde (Fig 4B) or 10% formalin (Fig 4C–G). H & E staining of jejunum cross-sections (Fig 4B–C) and immunofluorescence staining of livers (Fig. 4d) were made from mice that received adenoviruses expressing mouse IgG Fc (Fc) or different Fz-subtype-specific DRPB antagonist, 7 days post adenovirus injection (n=6 to n=9 mice/group). Paraffin-embedded sections were stained with mouse anti-glutamine synthetase (GS) antibody (Millipore #MAB302, 1:50) following citrate antigen retrieval and blocking with 5% normal goat serum. The immunostained tissue sections were analyzed and images were captured on a fluorescence microscope (KEYENCE BZ-X710). For GS quantification, 3 pictures at 10 magnification from each section were analyzed using Image J, quantifying the integrated density of the area (100μm × 100μm) around the central vein. 4 areas were measured in each picture. The average of the integrated density was normalized by Ad-Fc control. All animal experiments were conducted in accordance with procedures approved by the IACUC at Stanford University. Serum expression of Ad-Fz-subtype-specific DRPB antagonists (DRPB_Fz4, Fz7, Fz8 and Fz7/8) were confirmed by immunoblotting using mouse anti-6 × His (Abcam ab18184). All experiments used n = 6 to n = 9 mice per group and were repeated twice. All animal experiments were conducted in accordance with procedures approved by the IACUC at Stanford University.

Mouse liver RNA isolation, cDNA synthesis, and qPCR

A small portion of liver from each mouse was cut and placed in RNAlater (Invitrogen). Total RNA was isolated using TRIzol Reagent (Life Technologies) and Direct-Zol MiniPrep Kit (Zymo). cDNA was generated from 500ng of RNA using iScript™ Reverse Transcription Supermix for RT-qPCR (Bio-Rad). qPCR was performed on a total of 5.6ng of cDNA per sample using Power SYBR™ Green PCR Master Mix (Applied Biosystems) on the CFX384 Real-Time System (Bio-Rad). Fold changes in gene expression were calculated using the Ct

method from Ct values normalized to Gapdh on Microsoft Excel and PRISM. Primer sequences for each gene were published as follows:

Mouse GS F - 5′-ATGCAGATAGGGTGACCACT-3′

Mouse GS R - 5′-GTCCATTTGCAGGAAATGGC-3′

Mouse Axin2 F - 5′-GCAGGAGCCTCACCCTTC-3′

Mouse Axin2 R - 5′-TGCCAGTTTCTTTGGCTCTT-3′

Mouse Gapdh F - 5′-CCCCAATGTGTCCGTCGTG-3’

Mouse Gapdh R - 5′-GCCTGCTTCACCACCTTCT-3′

Statistical Analysis

Statistical analysis was performed using the GraphPad Prism software. All statistical tests use biological replicates and are indicated by group size (n) in figure legend. Results were expressed as mean ± s.e.m. (standard error of mean). Two-sided P-values were calculated by Dunn’s test of multiple comparisons following Kruskal-Wallis test. *P<0.05; ** P<0.01, ****P<0.0001.

Reporting Summary statement: Further information on experimental design is available in the Nature Research Reporting Summary linked to this article.

Data Availability Statement: The structures are deposited in Protein Data Bank under the accession codes 6NDZ, 6NE1, 6NE2 and 6NE4. Other data are available from corresponding authors upon reasonable requests.

Supplementary Material

Refer to Web version on PubMed Central for supplementary material.

Acknowledgments:

We thank Andrew Velasco and Deepa Waghray for assistance. GM/CA@APS has been funded in whole or in part with Federal funds from the National Cancer Institute (ACB-12002) and the National Institute of General Medical Sciences (AGM-12006). This research used resources of the Advanced Photon Source, a U.S. Department of Energy (DOE) Office of Science User Facility operated for the DOE Office of Science by Argonne National Laboratory under Contract No. DE-AC02–06CH11357. The Eiger 16M detector was funded by an NIH–Office of Research Infrastructure Programs, High-End Instrumentation Grant (1S10OD012289–01A1). The Berkeley Center for Structural Biology is supported in part by the Howard Hughes Medical Institute. The Advanced Light Source is a Department of Energy Office of Science User Facility under Contract No. DE-AC02–05CH11231. Use of the Stanford Synchrotron Radiation Lightsource, SLAC National Accelerator Laboratory, is supported by the U.S. Department of Energy, Office of Science, Office of Basic Energy Sciences under Contract No. DE-AC02–76SF00515. The SSRL Structural Molecular Biology Program is supported by the DOE Office of Biological and Environmental Research, and by the National Institutes of Health, National Institute of General Medical Sciences (including P41GM103393).

The work here is supported by Ludwig Foundation, Mathers Fund and HHMI (K.C.G.); HHMI (D.B.); NIH grants U01DK085527, U19AI116484, R01NS100904 and U01CA217851 (C.J.K.); NIH grant 1R01DK115728 (C.J.K. and K.C.G.).

References:

1. Davis MI et al. Comprehensive analysis of kinase inhibitor selectivity. Nature biotechnology 29, 1046 (2011).
2. Massague J TGF-beta signal transduction. Annu. Rev. Biochem 67, 753–791, doi:10.1146/annurev.biochem.67.1.753 (1998). [PubMed: 9759503]
3. Luca VC et al. Structural basis for Notch1 engagement of Delta-like 4. Science 347, 847–853 (2015). [PubMed: 25700513]
4. Artavanis-Tsakonas S, Rand MD & Lake RJ Notch signaling: cell fate control and signal integration in development. Science 284, 770–776 (1999). [PubMed: 10221902]
5. Mendoza JL et al. The IFN-λ-IFN-λR1-IL-10Rβ complex reveals structural features underlying type III IFN functional plasticity. Immunity 46, 379–392 (2017). [PubMed: 28329704]
6. Spangler JB, Moraga I, Mendoza JL & Garcia KC Insights into cytokine–receptor interactions from cytokine engineering. Annual review of immunology 33, 139–167 (2015).
7. Kummer L et al. Structural and functional analysis of phosphorylation-specific binders of the kinase ERK from designed ankyrin repeat protein libraries. Proceedings of the National Academy of Sciences 109, E2248–E2257 (2012).
8. Schilling J, Schöppe J & Plückthun A From DARPins to LoopDARPins: novel LoopDARPin design allows the selection of low picomolar binders in a single round of ribosome display. Journal of molecular biology 426, 691–721 (2014). [PubMed: 24513107]
9. Binz HK et al. High-affinity binders selected from designed ankyrin repeat protein libraries. Nature biotechnology 22, 575 (2004).
10. Plückthun A Designed ankyrin repeat proteins (DARPins): binding proteins for research, diagnostics, and therapy. Annual review of pharmacology and toxicology 55, 489–511 (2015).
11. Nusse R & Clevers H Wnt/β-Catenin Signaling, Disease, and Emerging Therapeutic Modalities. Cell 169, 985–999 (2017). [PubMed: 28575679]
12. Reya T & Clevers H Wnt signalling in stem cells and cancer. Nature 434, 843 (2005). [PubMed: 15829953]
13. Clevers H Wnt/β-catenin signaling in development and disease. Cell 127, 469–480 (2006). [PubMed: 17081971]
14. Gurney A et al. Wnt pathway inhibition via the targeting of Frizzled receptors results in decreased growth and tumorigenicity of human tumors. Proceedings of the National Academy of Sciences 109, 11717–11722 (2012).
15. Janda CY, Waghray D, Levin AM, Thomas C & Garcia KC Structural basis of Wnt recognition by Frizzled. Science, 1222879 (2012).
16. Rohl CA, Strauss CE, Misura KM & Baker D in Methods in enzymology Vol. 383 66–93 (Elsevier, 2004). [PubMed: 15063647]
17. Fallas JA et al. Computational design of self-assembling cyclic protein homo-oligomers. Nature chemistry 9, 353 (2017).
18. Boder ET & Wittrup KD Yeast surface display for screening combinatorial polypeptide libraries. Nature biotechnology 15, 553 (1997).
19. Whitehead TA et al. Optimization of affinity, specificity and function of designed influenza inhibitors using deep sequencing. Nature biotechnology 30, 543 (2012).
20. Janda CY et al. Surrogate Wnt agonists that phenocopy canonical Wnt and β-catenin signalling. Nature 545, 234–237 (2017). [PubMed: 28467818]
21. Yan KS et al. Non-equivalence of Wnt and R-spondin ligands during Lgr5+ intestinal stem-cell self-renewal. Nature 545, 238–242 (2017). [PubMed: 28467820]
22. Kuhnert F et al. Essential requirement for Wnt signaling in proliferation of adult small intestine and colon revealed by adenoviral expression of Dickkopf-1. Proceedings of the National Academy of Sciences 101, 266–271 (2004).
23. Kabiri Z et al. Stroma provides an intestinal stem cell niche in the absence of epithelial Wnts. Development, dev. 104976 (2014).

24. Wei K et al. A liver Hif-2α–Irs2 pathway sensitizes hepatic insulin signaling and is modulated by Vegf inhibition. Nature medicine 19, 1331 (2013).
25. van Es JH et al. Wnt signalling induces maturation of Paneth cells in intestinal crypts. Nature cell biology 7, 381 (2005). [PubMed: 15778706]
26. Benhamouche S et al. Apc tumor suppressor gene is the "zonation-keeper" of mouse liver. Developmental cell 10, 759–770 (2006). [PubMed: 16740478]
27. Liu CQ, Bakeri H, Li TS & Swaroop A Regulation of retinal progenitor expansion by Frizzled receptors: implications for microphthalmia and retinal coloboma. Hum. Mol. Genet 21, 1848–1860, (2012). [PubMed: 22228100]

Methods-only References:

28. Janda CY et al. Surrogate Wnt agonists that phenocopy canonical Wnt and beta-catenin signalling. Nature 545, 234–237, (2017). [PubMed: 28467818]
29. Gurney A et al. Wnt pathway inhibition via the targeting of Frizzled receptors results in decreased growth and tumorigenicity of human tumors. Proc. Natl. Acad. Sci. U. S. A 109, 11717–11722, (2012). [PubMed: 22753465]
30. Kabsch W Integration, scaling, space-group assignment and post-refinement. Acta Crystallographica Section D: Biological Crystallography 66, 133–144 (2010). [PubMed: 20124693]
31. Otwinowski Z & Minor W in Methods in enzymology Vol. 276 307–326 (Elsevier, 1997).
32. Janda CY, Waghray D, Levin AM, Thomas C & Garcia KC Structural Basis of Wnt Recognition by Frizzled. Science 337, 59–64, (2012). [PubMed: 22653731]
33. Emsley P, Lohkamp B, Scott WG & Cowtan K Features and development of Coot. Acta Crystallographica Section D: Biological Crystallography 66, 486–501 (2010). [PubMed: 20383002]
34. Afonine PV et al. Towards automated crystallographic structure refinement with phenix. refine. Acta Crystallographica Section D: Biological Crystallography 68, 352–367 (2012). [PubMed: 22505256]
35. Sato T et al. Single Lgr5 stem cells build crypt-villus structures in vitro without a mesenchymal niche. Nature 459, 262–265, (2009). [PubMed: 19329995]

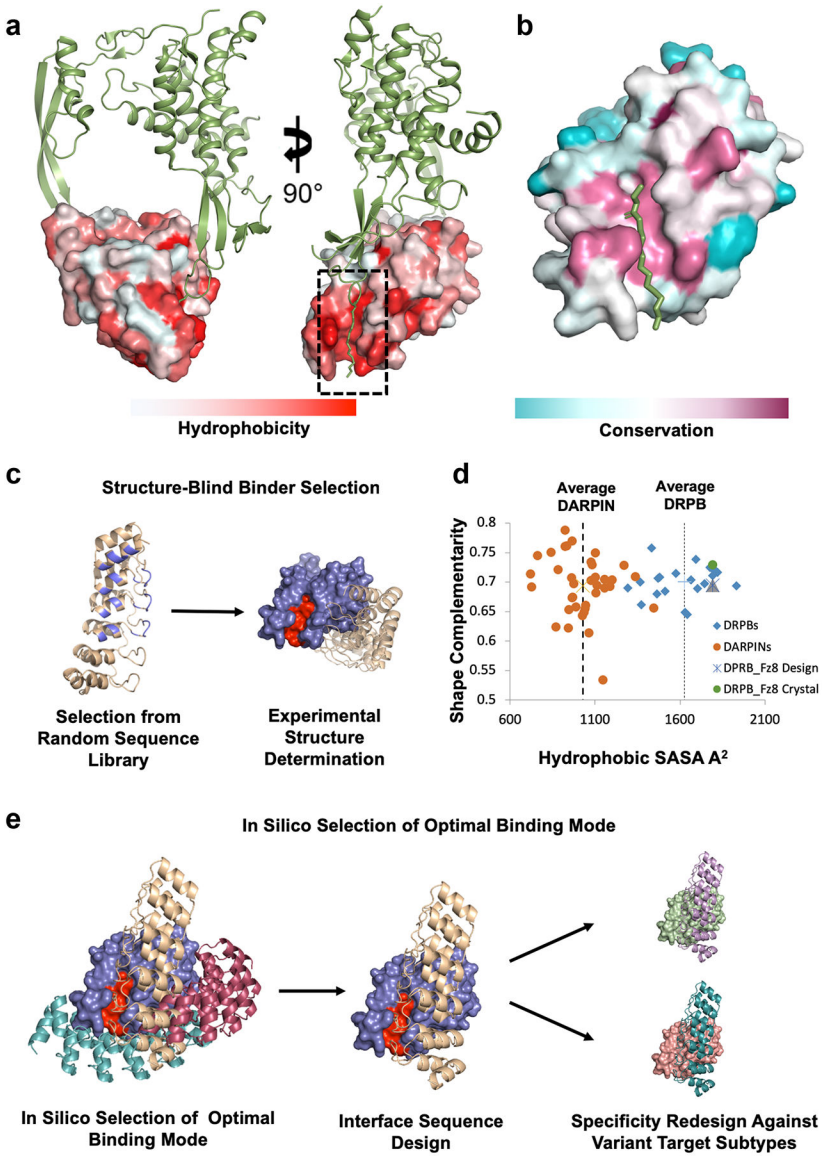

Fig. 1.

Computational design of Fz-subtype specific designed repeat protein binders (DRPBs). **a,** Native XWnt8 (green)-Fz8CRD (colored by hydrophobicity) complex depicting the essential functional interaction: deep insertion of the Wnt lipid group (sticks) into the Fz hydrophobic lipid binding groove. **b,** Structure of 6 human Fz CRDs colored by conservation, with the highest conservation colored in magenta as seen in the Fz essential hydrophobic groove, adjacent positions are less well conserved. **c,e,** Differences between *in silico* method for selecting binding modes for designed repeat protein binders (DRPBs) versus binder selection from randomized libraries. Traditional, empiric methods (c) mutagenize scaffold surface residues, select the randomized library for binding (c, left), and then experimentally determine the binding mode after maturation (c, right), often revealing a binding footprint incompatible with functional activity. In the computational, structure-guided design of DRPBs (e), optimal backbone conformations are discovered by exhaustive

computational docking of a scaffold (ankyrin) against the target (blue). Optimal shape complementary binding modes are rationally selected to maximize functional blockade and include extensive coverage of adjacent variant regions (e, left). The interface of the selected binding mode is then computationally optimized (e, middle). Further redesign generate orthogonal subtype specificities are engineered via substitution of the target structure with related structures and subsequent redesign (e, right). **d,** DRPBs (dotted line) generated with this computational approach have significantly larger hydrophobic buried surface area than typical monomeric DARPIN interfaces (dashed line), but notably retain similar shape complementary across these larger interfaces.

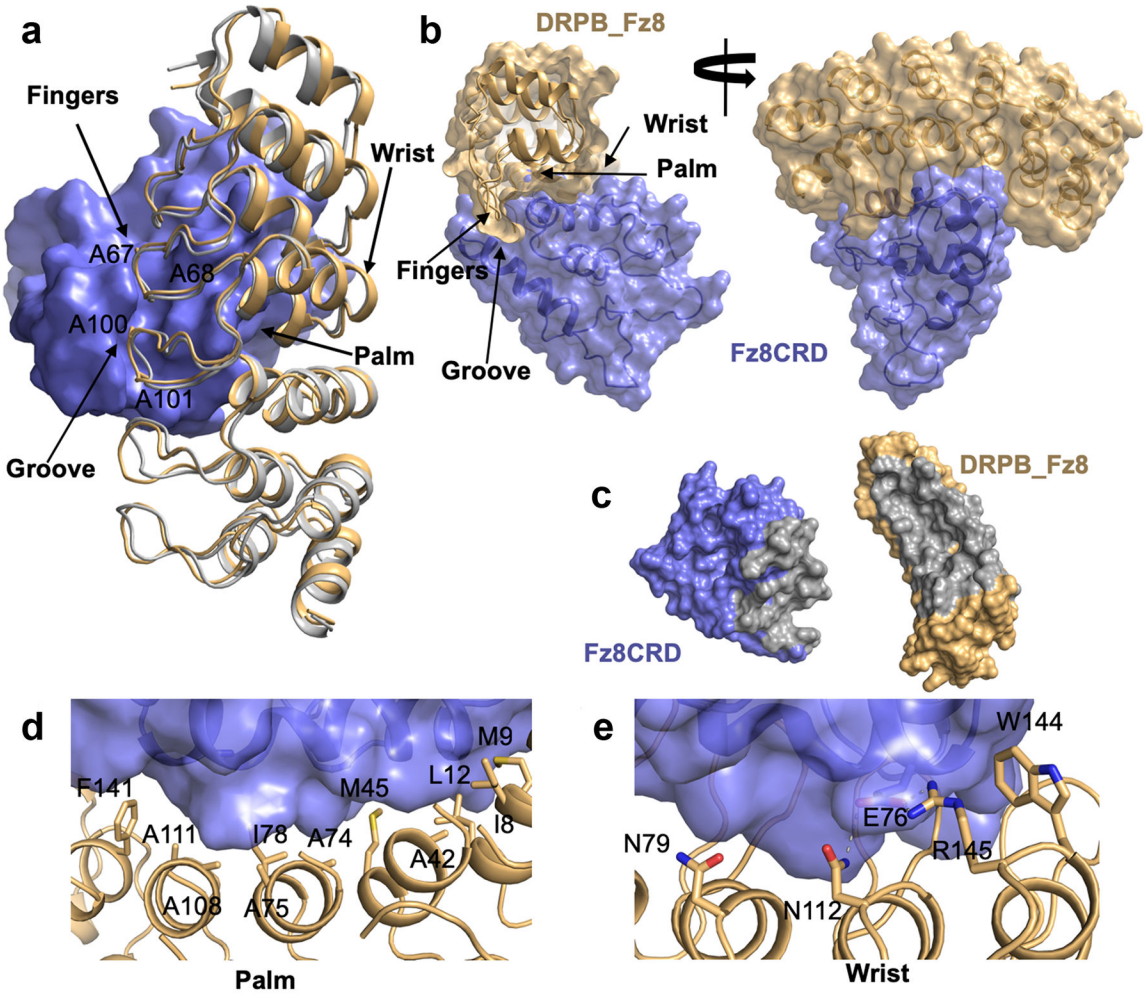

Fig. 2.

DRPB_Fz8-Fz8CRD complex structure confirms computational design and paves the way for specificity tuning.

a, Crystal structure of DRPB_Fz8-Fz8CRD matches the computationally designed complex. The Fz8CRD is shown by blue surface. The crystal complex DRPB_Fz8 is colored in light orange and the computational model is colored in grey. The Ala “fingers” of DRPB_Fz8 are deeply “grasping” the hydrophobic groove of Fz8CRD. **b,** Overall structures of DRPB_Fz8 with Fz8CRD. **c,** An “open-book” view showing the interacting surface on both Fz8CRD and DRPB_Fz8. The interacting surface on Fz8CRD and DRPB_Fz8 is colored in grey. **d,** The “palm” region of DRPB_Fz8 consists of hydrophobic residues that make van der Waals interactions with Fz8 CRD. The “fingers” region of DRPB_Fz8 is omitted to gain a clear view. **e,** The “wrist” region of DRPB_Fz8 consists of hydrophilic and charged residues that contribute to both solubility and receptor recognition. The DRPB_Fz8 Asn112 and Arg145 form hydrogen bonds and salt bridges with Glu76 of Fz8CRD, shown as grey dashed lines.

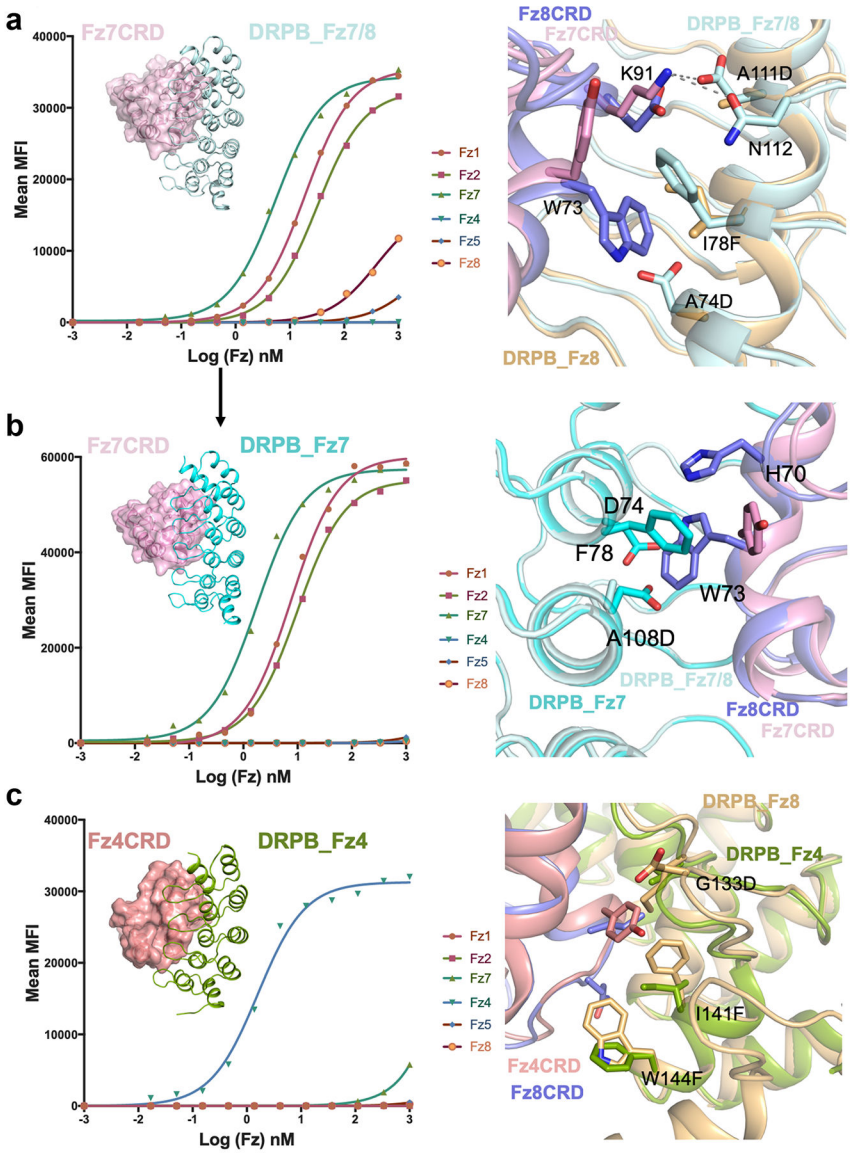

Fig. 3.

Complex structures of DRPB-Fz explain Fz subtype specificity.

a, Titration of DPRB_Fz7/8 to biotinylated Fz 1/2/4/5/7/8 CRDs. DPRB_Fz8 was expressed on yeast surface. Biotinylated Fz 1/2/4/5/7/8 was added at gradient concentration. Alexa Fluor® 647 streptavidin was subsequently added and the median fluorescence intensity (MFI) was analyzed and plotted in Prism 7. DPRB_Fz7/8 showed EC_{50} of 19.0, 31.6 and 5.6 nM to Fz1, 2 and 7. DPRB_Fz7/8 showed weaker staining to Fz5/8 with EC_{50} not available. Representative Ala111Asp mutation from DPRB_Fz8 to DPRB_Fz7/8 allows hydrogen bond and salt bridge formation between DPRB_Fz7/8 with Fz7 Lys91, shown by grey dashed lines. DPRB_Fz7/8 is colored in pale cyan. Fz7CRD is colored in pink and Fz8CRD is colored in slate. The corresponding position of Lys91 is Glu, weakening DPRB_Fz7/8 interaction with Fz8 subtype. **b,** DPRB_Fz7 showed strong binding to Fz1, 2 and 7, respectively. DPRB_Fz7 showed no cross-reactivity to Fz5/8 up to 1 uM concentration

(Table Supplementary Notes, page 5). The Ala108Asp mutation from DPRB_Fz7/8 to DPRB_Fz7 leads to steric clashes with Trp73 of Fz8 CRD. On the other hand, the corresponding position of Fz7 subtype is Tyr, whose less bulky sidechain allows it take a different rotamer conformation. This Ala108Asp mutation thus further confers specificity to Fz7 subtype by eliminating Fz8 binding. DPRB_Fz7/8 here is colored in light cyan while DPRB_Fz7 is colored in cyan. **c,** DPRB_Fz4 only binds to Fz4 with EC_{50} of 1.6 nM. DPRB_Fz4-Fz4CRD showed backbone movement compared with DPRB_Fz8-Fz8CRD. Therefore, DPRB_Fz4 and Fz4CRD were individually superpositioned with DPRB_Fz8 and Fz8CRD. The differences between DPRB_Fz4 and DPRB_Fz8 surface lead to less favorable interactions between DPRB_Fz4 with Fz8. For examples, Asp133Gly, Phe141Ile and Trp144Phe weaken interactions to Fz8CRD due to less bulky sidechains. The yeast titration experiements were repeated once with similar results.

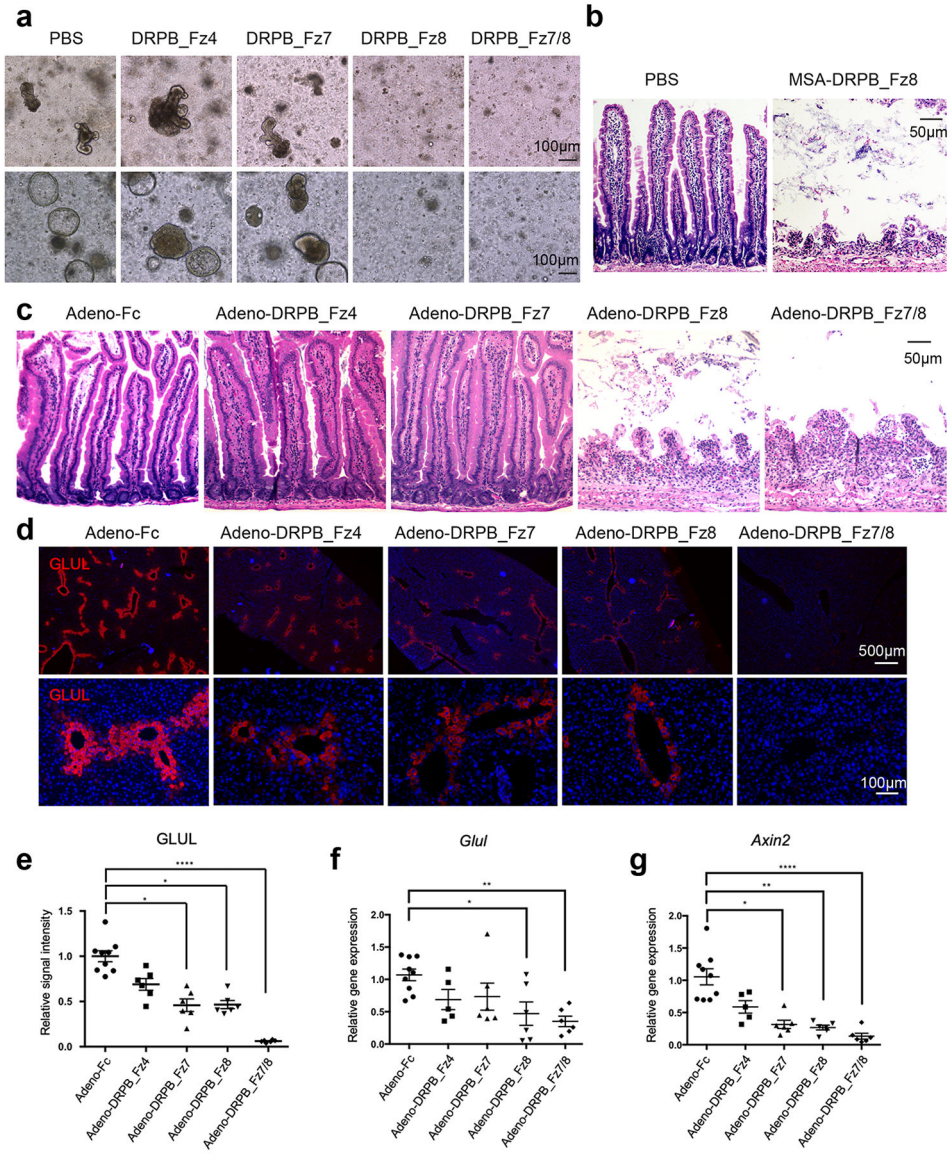

Fig. 4.

Fz-subtype specific DRPB antagonists inhibit homeostasis of the intestinal crypt stem cell compartment and expression of liver Wnt target genes.

a, Mouse (top) and human (bottom) primary duodenal organoids which endogenously produce Wnt were cultured in submerged Matrigel in medium containing ENR (EGF/Noggin/R-spondin) with different Fz-subtype-specific DRPB antagonist at 100 nM. The images were taken at day 7 (mouse) or day 10 (human) of continuous DRPB antagonist exposure. Each Fz antagonist was replenished every 3 days during medium change. *In vitro* experiments were repeated at least three times, and representative images are shown. **b,** *In vivo* phenotype following daily intravenous (i.v.) injections of recombinant MSA-DRPB_Fz8 at a concentration of 20mg/kg or PBS for 7 days. H & E staining of jejunum is shown. The experiment was performed once due to limited protein yield. **c-d,** Representative images of H & E staining of jejunum cross-sections (**c)** and glutamine synthetase (GLUL,

pericentral marker) immunofluorescence staining of livers (**d)** from mice that received adenoviruses expressing negative control IgG2a Fc (Fc) or different Fz-subtype-specific DRPB antagonist, 7 days post adenovirus injection (representative images from n=6 to n=9 mice/group. Experiments were repeated twice). **e,** Quantification of the GLUL immunofluorescence signal intensity shown in (D). **f-g,** Quantification of the *Glul* **(f)** and *Axin2* **(g)** transcript levels relative to GAPDH from liver samples (**d**) by qRT-PCR. Statistical analysis was performed using GraphPad Prism software. Data represent mean ± s.e.m. (n=9; control and n=6; other groups biological replicates from 2 experiments; for all in vivo experiments (panels c-g)) Two-sided P-values were calculated by Dunn's test of multiple comparisons following Kruskal-Wallis test. *P < 0.05; **P < 0.01; ****P < 0.0001.

Table 1

Data collection and refinement statistics (molecular replacement)

	DRPB_Fz8 + Fz8 CRD (PDB 6NDZ)	DRPB_Fz7/8 + Fz7 CRD (PDB 6NE2)	DRPB_Fz4 + Fz4 CRD (PDB 6NE1)	DRPB_Fz7 + Fz7 CRD (PDB 6NE4)
Data collection				
Space group	P 2_1 2_1 2_1	P 2 2_1 2_1	P 2 2_1 2_1	P 2 2_1 2_1
Cell dimensions				
a, *b*, *c* (Å)	79.9, 109.0, 114.4	57.6, 68.0, 86.4	51.8, 62.6, 86.2	57.6, 68.4, 86.5
α, *β*, *γ*(°)	90, 90, 90	90, 90, 90	90, 90, 90	90, 90, 90
Resolution (Å)	50.0–2.22 (2.26–2.22)[a]	45.0–1.30 (1.38–1.30)	50–3.00 (3.05–3.00)	50.0–1.65 (1.68–1.65)
R_{merge}	0.14 (0.92)	0.054 (0.65)	0.16 (0.82)	0.084 (0.72)
$I/\sigma(I)$	26.8 (1.2)	16.2 (1.4)	10.8 (1.0)	38.1 (2.3)
$CC_{1/2}$	1 (0.58)	1 (0.61)	1 (0.66)	1 (0.80)
Completeness (%)	93.5 (70.8)	99.0 (93.9)	99.0 (91.5)	99.8 (99.6)
Redundancy	10.5 (3.8)	7.0 (3.6)	5.6 (3.3)	11.9 (10.0)
Refinement				
Resolution (Å)	41.9–2.26 (2.35–2.26)	39.2–1.30 (1.35–1.30)	43.1–3.01 (3.12–3.01)	34.2–1.65 (1.71–1.65)
No. reflections	44466	83589	5863	41811
R_{work} / R_{free}	0.212/0.238	0.161/0.184	0.234/0.293	0.160/0.186
No. atoms				
Protein	7011	2368	2028	2358
Ligand/ion	56 (MPD, ACT, ACY)	108 (ACT, SO4, EDO, NAG)	28 (NAG)	78 (SO4, EDO)
Water	216	268	6	274
B factors				
Protein	73.5	23.2	74.9	28.5
Ligand/ion	90.6	42.1	116.9	62.9
Water	59.4	33.9	34.0	41.0
R.m.s. deviations				
Bond lengths (Å)	0.003	0.007	0.004	0.014
Bond angles (°)	0.94	0.97	1.02	1.33

6NDZ data is collected with 2 protein crystals and the others are collected on a single crystal.

[a]Values in parentheses are for highest-resolution shell.